Article

Generalized One-Pot Synthesis, Characterization, and Photocatalytic Activity of Hierarchical BiOX (X = Cl, Br, I) Nanoplate Microspheres

Xi Zhang, Zhihui Ai, Falong Jia, and Lizhi Zhang

J. Phys. Chem. C, **2008**, 112 (3), 747-753 • DOI: 10.1021/jp077471t

Generalized One-Pot Synthesis, Characterization, and Photocatalytic Activity of Hierarchical BiOX (X = Cl, Br, I) Nanoplate Microspheres

Xi Zhang, Zhihui Ai, Falong Jia, and Lizhi Zhang*

Key Laboratory of Pesticide & Chemical Biology of Ministry of Education, College of Chemistry, Central China Normal University, Wuhan 430079, People's Republic of China

Received: September 17, 2007; In Final Form: October 21, 2007

A general one-pot solvothermal process was explored to prepare BiOX (X = Cl, Br, I) powders by employing ethylene glycol as the solvent. The as-prepared BiOX powders were characterized by X-ray powder diffraction, scanning electron microscopy, transmission electron microscopy, high-resolution transmission electron microscopy, UV−vis diffuse reflectance spectroscopy, and nitrogen sorption. The resulting BiOX samples were phase-pure and of hierarchical microspheres consisting of nanoplates. The band gaps of the as-prepared powders were estimated to about 3.22, 2.64, and 1.77 eV for BiOCl, BiOBr, and BiOI, respectively. On the basis of characterization results, we proposed a possible process for the growth of hierarchical BiOX nanoplate microspheres. Moreover, we evaluated their photocatalytic activities on the degradation of methyl orange and compared them with TiO_2 (Degussa, P25) under UV−vis light irradiation and C-doped TiO_2 under visible light ($\lambda > 420$ nm) irradiation, respectively. It was found that all the BiOX samples were photocatalytically active and BiOI exhibited excellent activity under both UV−vis and visible light irradiation. The resulting hierarchical BiOX nanoplate microspheres are very promising photocatalysts for degrading organic pollutants and other applications.

1. Introduction

Since the development of materials with novel structures may open new opportunities in exploring their widely varying properties, the preparation of controlled structures has become an active research area in recent years. The arrangement of micro- and nanostructured building blocks (nanoparticles, nanorods, nanoribbons, and nanoplates) into hierarchical structures is of great interest to chemists and materials scientists. However, the direct fabrication of hierarchical nanostructures on the basis of the assembly of building blocks into three-dimensional (3D) ordered superstructures remains a challenge.[1−4] The major strategy to assembling hierarchical nanostructures is to first synthesize nanostructured building blocks and subsequently arrange these building blocks into hierarchical structures. Generally speaking, by concisely controlling the nucleation, and growth, followed by self-assembly, novel architectures with various surface structures can be achieved.

Numerous synthetic strategies have been developed to synthesize spatially patterned and controlled novel nanostructures. Among them, the solution process has proved to be a predominant synthetic approach. For example, hydrothermal and solvothermal processes are the most promising ones.[5] By regulating composition of solvents, reaction temperature, aging time, and additives, the crystalline phase, particle structure, and grain size could be well controlled during the hydrothermal or solvothermal process.[6−8] Polyol (such as ethylene glycol, diethylene glycol, and glycerol) process is a versatile chemical approach, which has successfully been used to prepare a great variety of nanostructured metals[9,10] and metal oxides.[11,12] Especially ethylene glycol (EG) has been found to be an attractive reaction medium because of its special physical and chemical properties. The high permittivity enables it to dissolve highly polar inorganic and organic compounds and to make the synthesis reactions achieved by the routes of highly polar or ionic intermediates, and the strong chelating ability makes it easy to form complexes with transition metal ions by using its hydroxyls as ligands so that some inorganic materials such as nitrates and halides can be dissolved in it to form a clear solution. Therefore, it often serves as a high-boiling solvent and a reducing agent, as well as a stabilizer to control particle growth.[13−15]

Bismuth oxyhalides, BiOX (X = Cl, Br, I), are of great importance because of their optical properties and promising industrial applications. All BiOX compounds crystallize in the tetragonal matlockite structure, a layer structure characterized by $[Bi_2O_2]$ slabs interleaved by double slabs of halogen atoms. Bismuth oxychloride is one of the simplest members of the Sillen family expressed by $[M_2O_2][Cl_m]$ or $[M_3O_{4+n}][Cl_m]$ ($m = 1-3$) where bismuth oxide based fluorite-like layers, $[M_2O_2]$ or $[M_3O_{4+n}]$, are intergrown with double chlorine layers.[16] These oxyhalide compounds can be applied as catalysts,[17,18] ferroelectric materials,[19,20] and pigments.[21] They can also be used as excellent photocatalysts to decompose organic compounds into inorganic substances for purifying textile dye polluted wastewater. For instance, Zhang and co-workers reported that BiOCl exhibited better performance than TiO_2 (P25, Degussa) on photocatalytic degradation of methyl orange (MO) dye.[22] Lin and co-workers reported that the photocatalytic activity of Bi_3O_4Cl, which was synthesized by a solid-state reaction of BiOCl and Bi_2O_3, was higher than that of anatase-type TiO_2 under UV light illumination for degrading MO.[23] Many solution routes have been applied to synthesize these compounds. For example, BiOCl powders were obtained via the hydrolysis method at room temperature,[22] or synthesized under hydrothermal conditions using hexadecylamine as organic template.[24]

* To whom correspondence should be addressed. Telephone/fax: +86-27-67867535. E-mail: zhanglz@mail.ccnu.edu.cn.

10.1021/jp077471t CCC: $40.75
Published on Web 01/03/2008

Very recently, reverse microemulsions consisting of heptane, nonionic surfactants, and aqueous salt solutions were used to synthesize BiOX nanoparticles.[25]

In this study, we report the first general one-pot solvothermal method to synthesize BiOX (X = Cl, Br, I) using ethylene glycol as the solvent. The as-prepared powders were microspheres with hierarchical superstructures. We studied how the solvent affected the formation of hierarchical microspheres. A possible mechanism for the formation of BiOX hierarchical microspheres in ethylene glycol under solvothermal conditions was proposed. Moreover, we evaluated photocatalytic activities of BiOX hierarchical microspheres on the degradation of methyl orange and compared them with TiO_2 (Degussa, P25) under UV−visible light and C-doped TiO_2 under visible light ($\lambda > 420$ nm) irradiation, respectively.

2. Experimental Section

2.1. Sample Preparation. The BiOX powders were synthesized by a simple soft chemical method. All the reagents were purchased from Sinopharm Chemical Reagent Co., Ltd. (Shanghai, China), and were used as received without further purification. In a typical synthesis, $Bi(NO_3)_3 \cdot 5H_2O$ (AR, 99.0%) was added slowly into an EG solution containing stoichiometric amounts of KCl (AR, 99.5%), NaBr (AR, 99.5%), and KI (AR, 98.5%) respectively, with the Bi/X molar ratio of 1. The mixture was stirred for 0.5 h at room temperature in air, and then poured into a 25 mL Teflon-lined stainless autoclave until 80% of the autoclave volume was filled. The autoclave was allowed to be heated at 160 °C for 12 h under autogenous pressure, and then air cooled to room temperature. The resulting precipitates were collected and washed with ethanol and deionized water thoroughly and dried at 50 °C in air. In order to understand the role of EG during synthesis, hydrothermal methods were also used to synthesize BiOX powders by replacing EG with water as the solvent.

Carbon-doped TiO_2 was synthesized by a hydrothermal method reported in our previous study.[30]

2.2. Characterization. X-ray powder diffraction (XRD) measurements of all the samples were performed in the reflection mode (Cu Kα radiation, $\lambda = 1.5418$ Å) on a Rigaku Ultima III X-ray diffractometer. The morphology and particle sizes were determined by a scanning electron microscopy (SEM, JEOL 6700-F). The samples for transmission electron microscopy (TEM) and high-resolution transmission electron microscopy (HRTEM) were prepared by dispersing the final powders in ethanol and the dispersion was dropped on carbon−copper grids. Then, the obtained powders deposited on a copper grid were observed by a high-resolution transmission electron microscope (JEOL JSM-2010) operating at 200 kV. UV−vis diffuse reflectance spectra (DRS) were obtained using a UV−vis spectrometer (Shimadzu UV-2550) by using $BaSO_4$ as a reference and were converted from reflection to absorbance by the Kubelka−Munk method.[31] Nitrogen adsorption−desorption isotherms were collected on a Micromeritics Tristar-3000 surface area and porosity analyzer at 77 K after the sample had been degassed in the flow of N_2 at 180 °C for 5 h. The BET surface area was calculated from the linear part of the BET plot ($P/P_0 = 0.1-0.25$).

2.3. Photocatalytic Activity Test. Photocatalytic activities of the BiOX powders were evaluated by the degradation of MO under UV−vis and visible light irradiation, respectively. In the case of visible light irradiation, the optical system used for the photocatalytic reaction consisted of a 500 W halogen−tungsten lamp and a 420 nm cutoff filter, which was placed under the reaction cell to completely remove all incoming wavelengths shorter than 420 nm to ensure irradiation with visible light only. All experiments were conducted at room temperature in air. In each experiment, 0.1 g of photocatalyst was added into 100 mL of MO solution with a concentration of 10 mg/L in a reaction cell with a Pyrex jacket. Prior to irradiation, the suspensions were stirred in the dark for 1 h to reach adsorption−desorption equilibrium. At irradiation time intervals of 1 h, 4 mL of the suspensions was collected and then the slurry samples including the photocatalyst and MO solution were centrifuged (12 000 rpm, 15 min) to remove the photocatalyst particles. The solutions were analyzed by a Hitachi U-3310 UV−visible spectrophotometer, and the absorbance at 464 nm was monitored. The photodegradation experiments under UV−vis light irradiation were similar to those under visible light without using a 420 nm cutoff filter. The average light intensity of the lamp was about 31.1 mW/cm^2 as measured by a light meter (Oriel, U.S.A.).

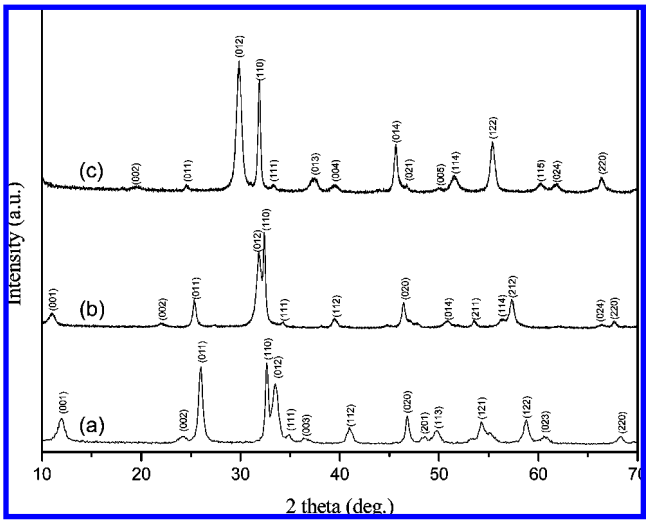

Figure 1. XRD patterns of as-prepared BiOX (X = Cl, Br, I) powders prepared by solvothermal process. (a) BiOCl, (b) BiOBr, and (c) BiOI.

3. Results and Discussion

3.1. Characterization of BiOX Samples. X-ray diffraction (XRD) was used to investigate the phase structures of the resulting powders. Figure 1 shows the XRD patterns of the as-prepared powders obtained from $Bi(NO_3)_3 \cdot 5H_2O$ with different alkali metal halides (KCl, NaBr, and KI) in ethylene glycol (EG). XRD analysis of the samples showed that all the powders were well crystallized. They can well be indexed to the hexagonal structures of BiOCl (JCPDS File No. 73-2060), BiOBr (JCPDS File No. 73-2061), and BiOI (JCPDS File No. 73-2062) for the samples synthesized in the presence of KCl, NaBr, and KI, respectively.

Figure 2 shows the SEM images of the as-prepared BiOX powders. Plenty of spherical superstructures were observed in all the products (Figure 2). The sizes of these spheres were not uniform. Their diameters were in the range of several micrometers to 10 μm. For instance, the diameters were about 1−3 μm for BiOCl, 2−10 μm for BiOBr, and 2−5 μm for BiOI, respectively. Higher magnification SEM images (inset of Figure 2) reveal the fine structures of BiOX. It was found that the BiOX microspheres were composed of nanoplates of about several nanometers in thickness. The nanoplates aligned radically and tightly to form hierarchical microspheres. Therefore, we conclude that this EG-based solvothermal process is a general approach to prepare hierarchical BiOX nanoplate microspheres.

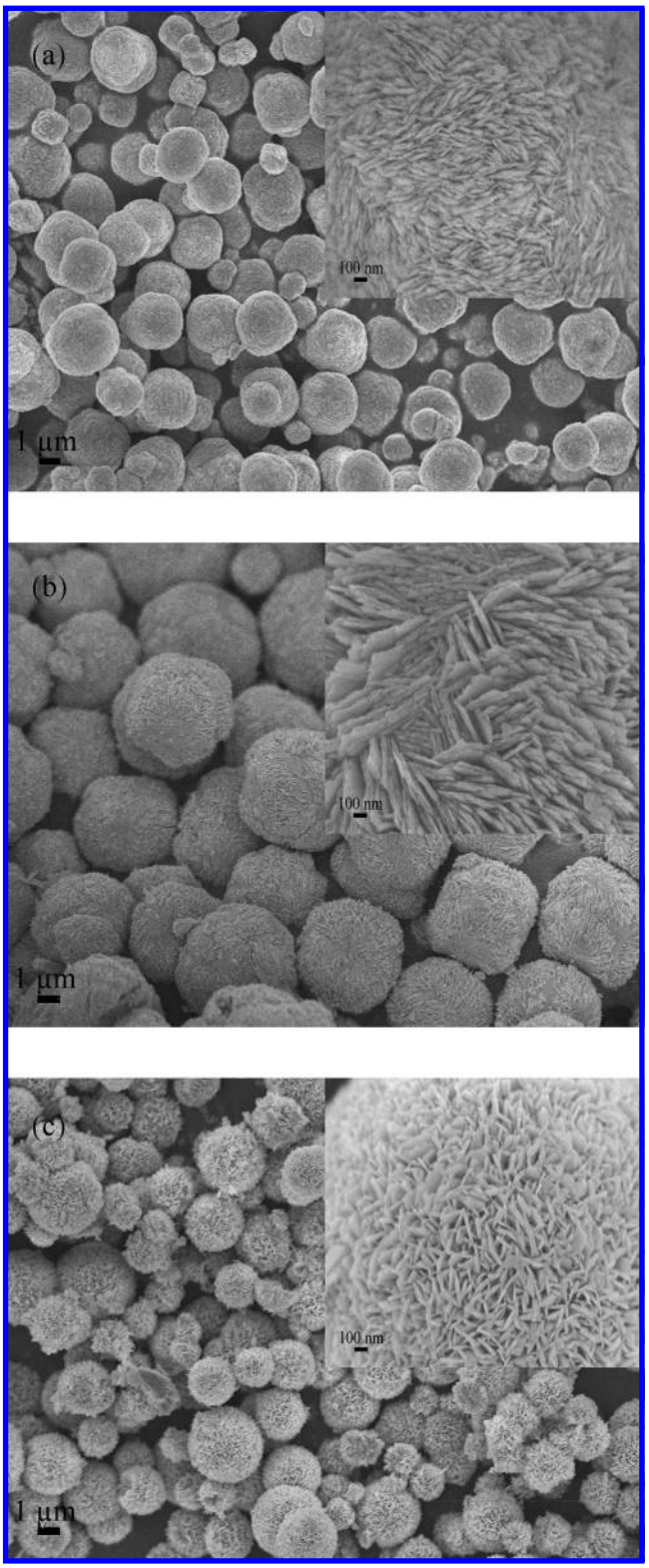

Figure 2. SEM images of as-prepared BiOX (X = Cl, Br, I) powders with inset showing a magnified view of the surface of microspheres. (a) BiOCl, (b) BiOBr, and (c) BiOI.

The obtained BiOX powders were further characterized by transmission electron microscopy (TEM). Figure 3 shows typical TEM images of BiOX powders. Irregular nanoplates are observed in the TEM images, which confirm that the as-synthesized microspheres are composed of platelike nanostructures. Figure 3a reveals the BiOCl nanoplates are about 8 nm in thickness. Figure 3b,c shows that BiOBr and BiOI are several tens to hundreds of nanometers in diameter. The BiOX

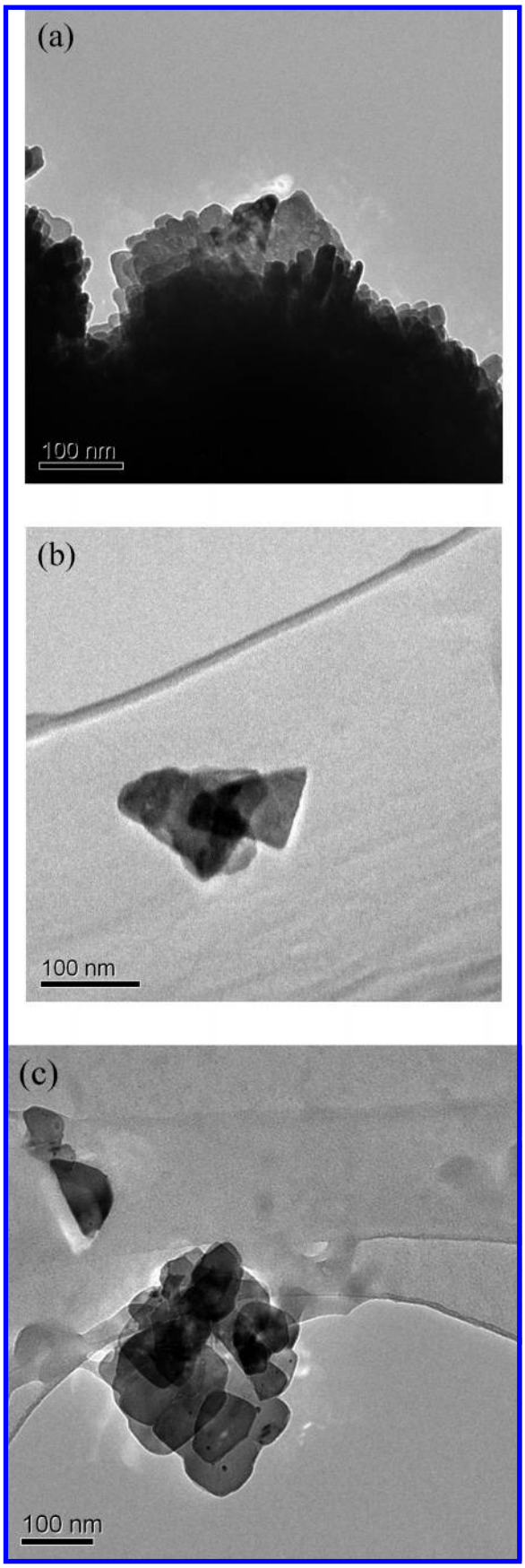

Figure 3. TEM images of as-prepared BiOX (X = Cl, Br, I) powders. (a) BiOCl, (b) BiOBr, and (c) BiOI.

nanoplates were further investigated by high-resolution transmission electron microscopy (HRTEM). As shown in Figure 4, clear lattice fringes can be observed and the single-crystal

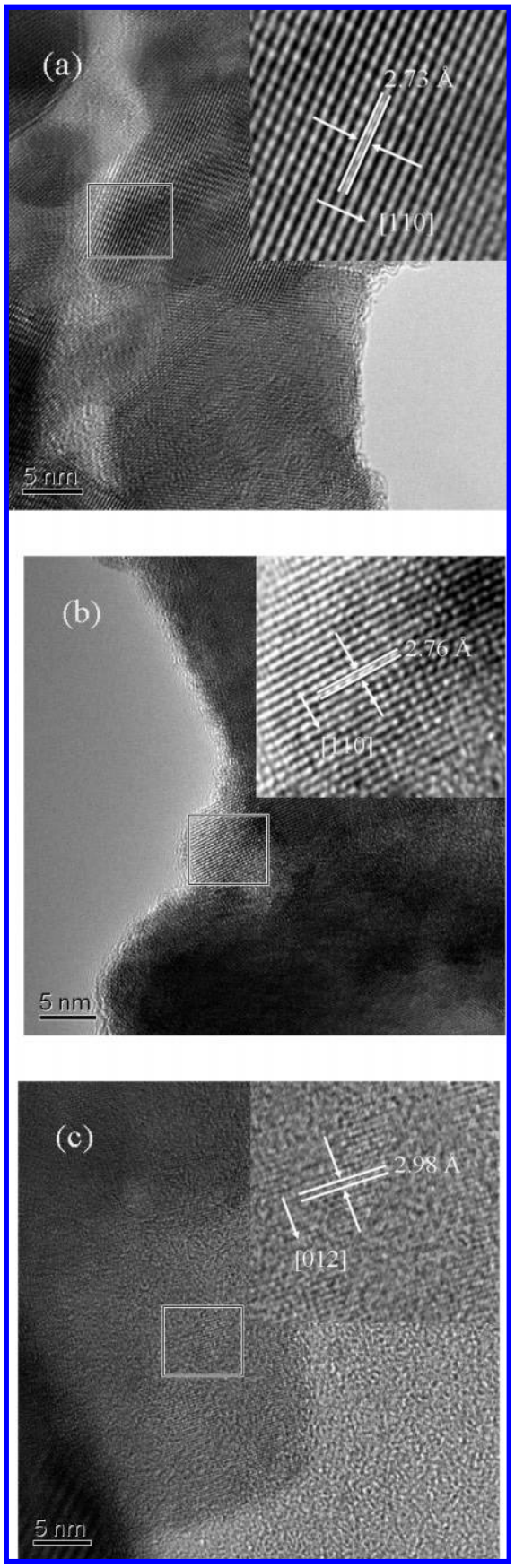

Figure 4. HRTEM images of as-prepared BiOX (X = Cl, Br, I) powders showing lattice fringes. (a) BiOCl, (b) BiOBr, and (c) BiOI.

natures of the nanoplates in the spherelike superstructures are revealed. Furthermore, the HRTEM images of BiOX powders are in good accordance with the result of XRD patterns shown in Figure 1. For example, the lattice spacing is about 2.73 Å between adjacent lattice planes of BiOCl (Figure 4a), which is consistent with the *d*-spacing of the [110] reflection (2.75 Å).

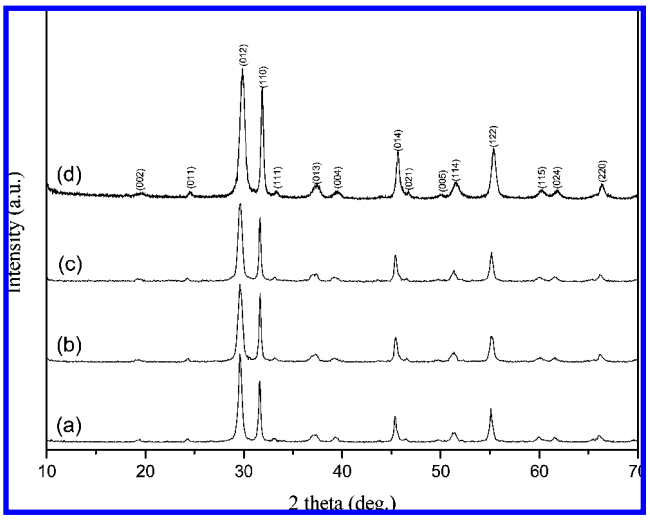

Figure 5. XRD patterns of BiOI powders collected at different reaction stages. (a) 0.5, (b) 3, (c) 6, and (d) 12 h.

3.2. Possible Formation Process of Hierarchical BiOX Nanoplate Microspheres. In order to understand the formation process of hierarchical BiOX nanoplate microspheres, time-dependent experiments were carried out and the resulting products collected at different stages were analyzed by XRD and SEM. Figure 5 are the XRD patterns of BiOI powders collected at different reaction stages, revealing that all the powders were well crystallized. All the observed patterns can be indexed to the tetragonal structure of BiOI (JCPDS File No. 73-2062). Figure 6 shows SEM images of BiOI powders collected at different reaction stages. Obviously, the reaction time has a significant influence on the morphologies of the obtained powders. On the basis of SEM images of the samples obtained at different stages, three formation stages could be identified. As shown in Figure 6a, as soon as BiOI nanoparticles formed in the early stage, they grew into nanoplates because of the directing ability of EG. Then, the BiOI nanoplates assembled together to form loosely attached aggregates with diameters of 2−4 μm (Figure 6b). With the reaction time increasing, the aggregates of nanoplates continuously grew to form microspheres (from Figure 6b to 6c) through a dissolution−recrystallization process of the preformed nanoparticles. After 12 h reaction, prefect hierarchical nanoplates microspheres were produced (Figure 6d).

We found that only large and thick BiOX plates were obtained instead of hierarchical nanoplate microspheres when we used the hydrothermal method to prepare BiOX by replacing EG with water as the solvent (Supporting Information). Therefore, the solvent EG plays an important role in the formation of the hierarchical BiOI nanoplate microspheres. Because of the special chemical and physical properties of EG, such as basicity, chelation, vapor pressure, viscosity, and so on, they can direct the crystal growth of BiOX. Considering the effects of hydrogen bonds between hydroxyl groups, EG molecules could exist in long chains.[26−28] Therefore, besides as the solvent, we believe EG also functions as a soft template, directing the growth of BiOX nanoparticles into nanoplates, and then inducing the formation of spherelike superstructures from these nanoplates during the synthesis.

On the basis of the above results, here we may propose the formation process of hierarchical BiOX nanoplate microspheres

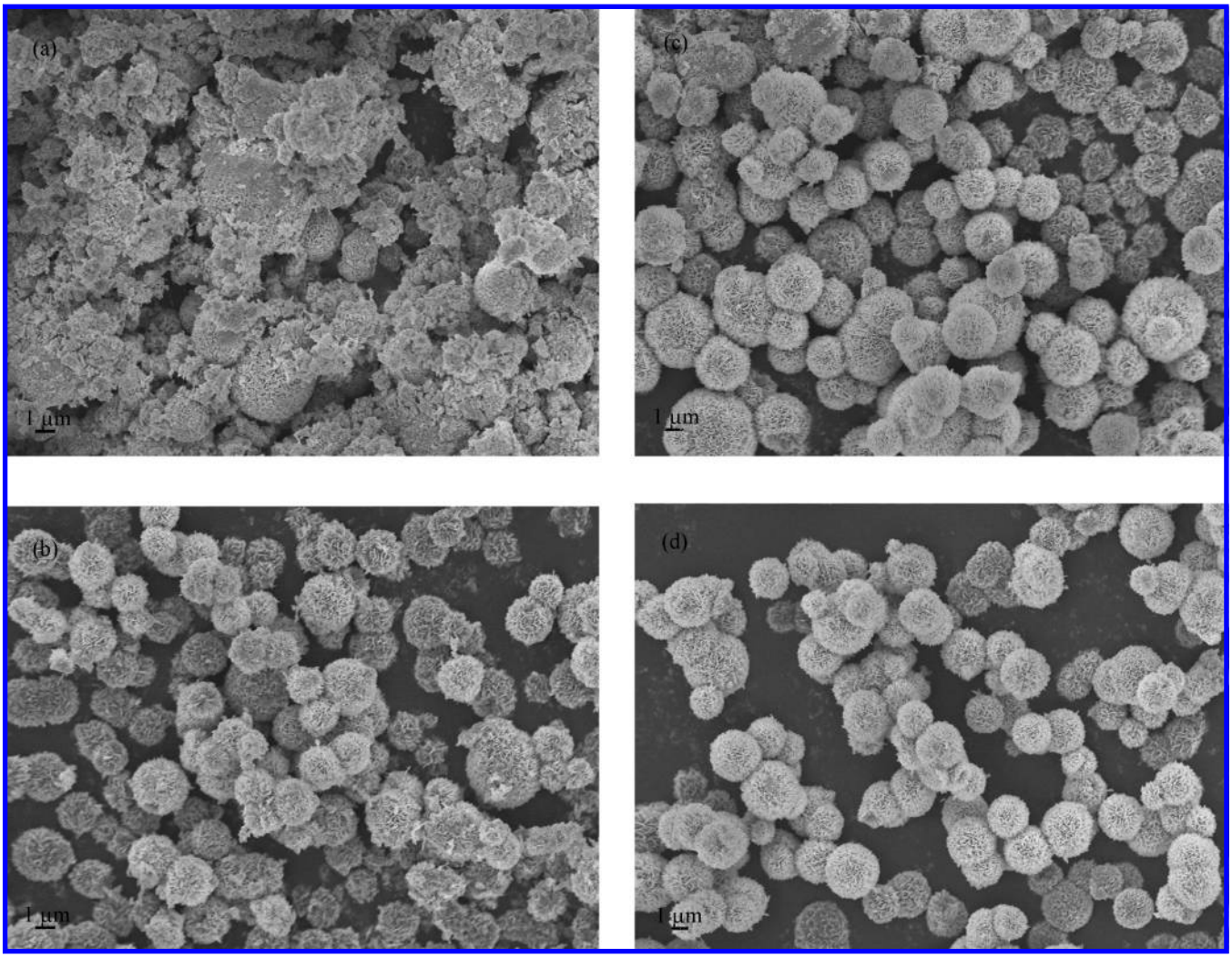

Figure 6. SEM images of BiOI powders collected at different reaction stages. (a) 0.5, (b) 3, (c) 6, and (d) 12 h.

SCHEME 1: Illustration of Possible Formation Mechanism of Hierarchical BiOX (X = Cl, Br, I) Nanoplate Microspheres[a]

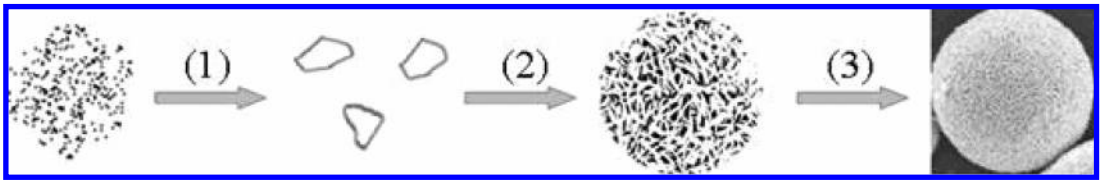

[a] (1) Formation of BiOX nanoparticles and their growth into nanoplates at the early stage. (2) EG-induced self-assembly of these primary nanoplates to form loose microspheres. (3) Formation of regular hierarchical microspheres through a dissolution−recrystallization process of the preformed nanoparticles.

(Scheme 1). It might be divided into three steps in sequence: (1) the formation of BiOX nanoparticles and their growth into nanoplates at the early stage; (2) EG-induced self-assembly of these primary nanoplates to form loose microspheres; (3) the formation of regular hierarchical microspheres through a dissolution−recrystallization process of the preformed nanoparticles. The detailed formation mechanism of BiOX in this EG solvothermal process needs further investigation.

3.3. Optical Absorption Properties and BET Surface Areas of BiOX Powders. UV−vis diffuse reflectance spectra (DRS) of the BiOX powders are shown in Figure 7. It is found that the absorption edges of the different BiOX samples are quite different. The UV−vis absorption edges of BiOX powders have a clear red shift with increasing X atomic numbers in sequence. The BiOCl and BiOBr powders have intense absorption edges at about 370 and 440 nm in the near-UV and visible light regions, respectively. BiOI powders have obvious absorption edges at about 670 nm in the visible light region. These results are consistent with the white, light yellow, and carmine red colors of BiOCl, BiOBr, and BiOI powders, respectively.

As a crystalline semiconductor, the optical absorption near the band edge follows the formula $\alpha h\nu = A(h\nu - E_g)^{n/2}$, where α, ν, E_g, and A are the absorption coefficient, light frequency, band gap energy, and a constant, respectively.[29] Among them, n depends on the characteristics of the transition in a semiconductor, i.e., direct transition ($n = 1$) or indirect transition ($n = 4$). For BiOX, the value of n is 4 for the indirect transition.[22] The band gap energies (E_g values) of BiOX can be thus

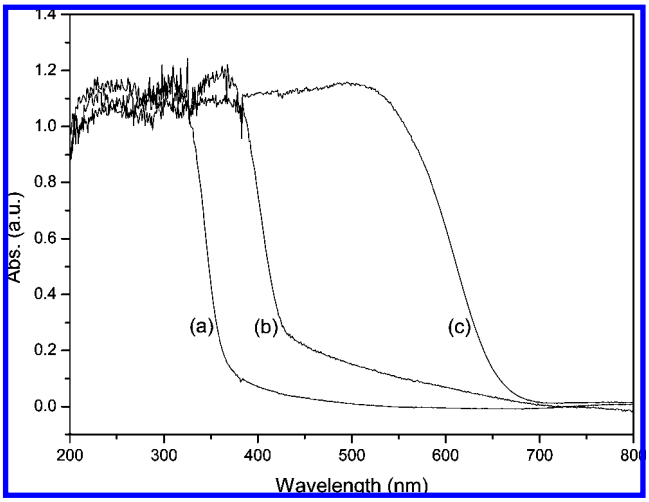

Figure 7. UV−vis diffuse reflectance spectra (DRS) of BiOX (X = Cl, Br, I) powders. (a) BiOCl, (b) BiOBr, and (c) BiOI.

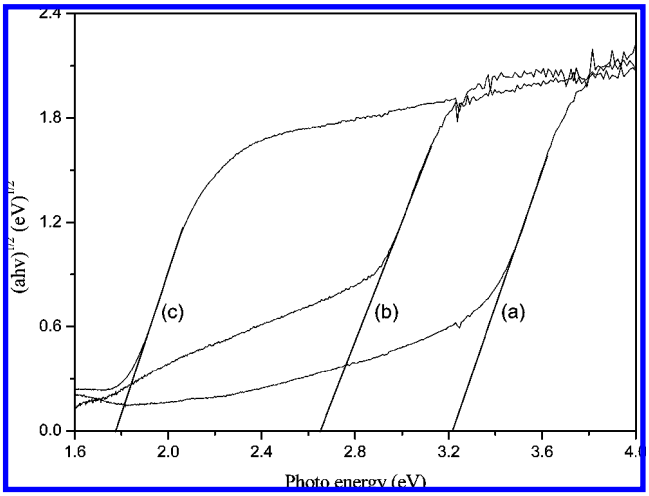

Figure 8. Plots of $(\alpha h\nu)^{1/2}$ vs photon energy ($h\nu$) for BiOX (X = Cl, Br, I) powders. (a) BiOCl, (b) BiOBr, and (c) BiOI.

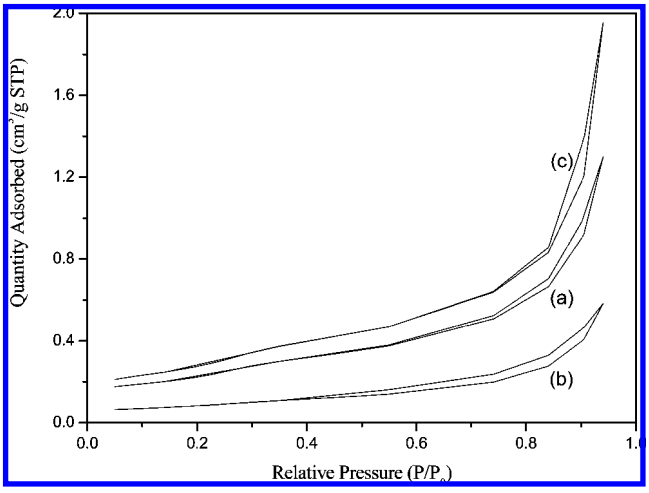

Figure 9. Nitrogen adsorption−desorption isotherms of BiOX (X = Cl, Br, I) powders. (a) BiOCl, (b) BiOBr, and (c) BiOI.

estimated from a plot of $(\alpha h\nu)^{1/2}$ versus photon energy ($h\nu$). The intercept of the tangent to the *x*-axis will give a good approximation of the band gap energies for the BiOX powders. Plots of $(\alpha h\nu)^{1/2}$ versus photon energy ($h\nu$) of BiOX powders are shown in Figure 8. The estimated band gap energies of the resulting samples were about 3.22, 2.64, and 1.77 eV for BiOCl, BiOBr, and BiOI, respectively, which are close to the values reported in the literature.[22,24,25] The band gap energies of BiOX were narrowed with increasing X atomic numbers in sequence.

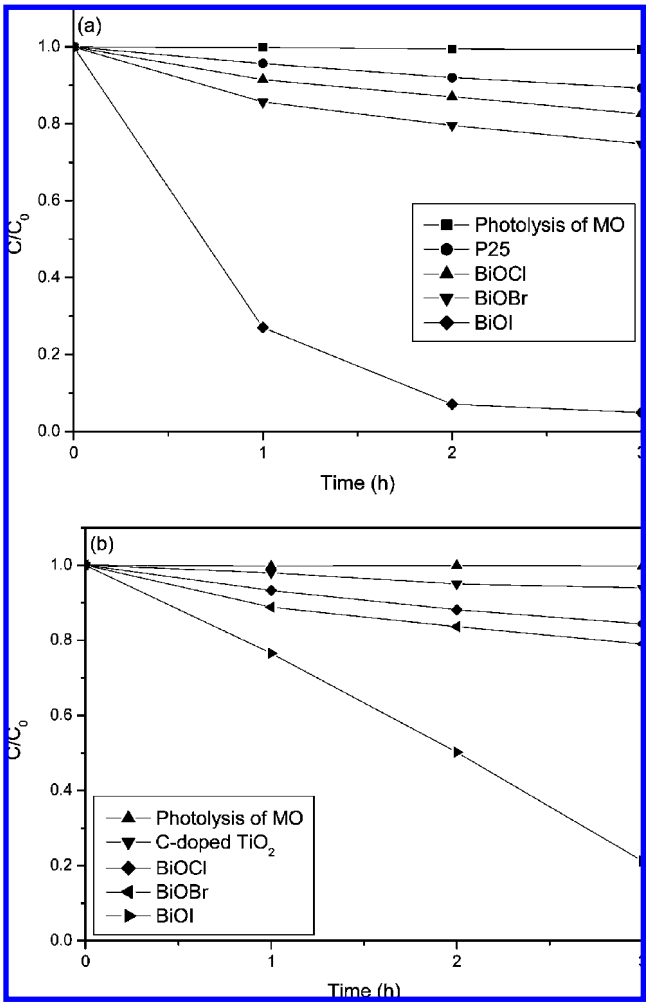

Figure 10. Photocatalytic degradation of MO in the presence of BiOX, P25, and C-doped TiO_2, and photolysis of MO. (a) Under UV−visible light irradiation and (b) under visible light irradiation.

TABLE 1: Textural Properties of BiOX (X = Cl, Br, I) Powders

	BiOCl	BiOBr	BiOI
A_{BET} ($m^2\ g^{-1}$)	18.3	6.8	22.7
V_{BJH} ($cm^3\ g^{-1}$)	0.046	0.021	0.069

The microporous structures and Brunauer−Emmett−Teller (BET) specific surface areas of the resulting samples were studied by nitrogen sorption. Figure 9 displays type II adsorption−desorption isotherms of all the BiOX samples, which are typical characteristics of macroporous materials. These macropores were believed to be produced by interaggregated BiOX nanoplates in the microspheres. In the nitrogen adsorption−desorption isotherms, there is only one hysteresis loop, corresponding to the filling of larger textural mesopores produced by interaggregated nanoplates. This confirms the result of SEM in Figure 2. The Brunauer−Emmett−Teller (BET) specific surface areas and pore volumes of BiOX powders are summarized in Table 1.

3.4. Photocatalytic Activity of BiOX. The photocatalytic activities of BiOX samples were measured on the degradation of MO in water under UV−vis and visible light irradiation, respectively. Figure 10a represents the variation of MO con-

centration (C/C_0) with irradiation time over different BiOX catalysts under UV−vis light irradiation. As a comparison, direct photolysis of MO and TiO_2 (Degussa, P25) were also performed under identical conditions. We observed that direct photolysis of MO was negligible under both UV−vis and visible light irradiation. Under UV−visible light irradiation, the degradation of MO on BiOCl and BiOBr was about 17% and 25%, respectively. Interestingly, MO can be very effectively degraded in the presence of BiOI powders, and the degradation efficiency reached about 95% in 3 h for BiOI. All the degradation ratios of MO on BiOX were significantly higher than that on the famous photocatalyst P25, which only degraded about 10% of MO. We also evaluated photocatalytic activities of BiOX under visible light ($\lambda > 420$ nm) and compared their activities with a visible light active photocatalyst, C-doped TiO_2, reported in our previous study.[30] It was found that BiOX were also active to degrade MO under visible light (Figure 10b). BiOCl, BiBr, and BiOI could degrade 15%, 21%, and 80% of MO in 3 h under visible light irradiation, respectively. These degradation efficiencies are slightly lower than that under UV−visible light, but still much higher than that of C-doped TiO_2, which degraded only 6% of MO in 3 h. Therefore, BiOX are promising photocatalysts under both UV−vis and visible light irradiation, while BiOI exhibits the best photocatalytic activity among all the BiOX samples. The higher photocatalytic activity of BiOI is attributed to its smaller band gap.

Under the illumination of UV−vis and visible light irradiation and in the presence of the photocatalyts BiOX, the photodecomposition of the MO could proceed in both a photocatalytic pathway and a photosensitization pathway. Both of these processes are dependent on the photocatalytic activity of the BiOX. As stated before, the band gaps of the resulting BiOCl, BiOBr, and BiOI samples were estimated to be about 3.22, 2.64, and 1.77 eV, respectively. Therefore, visible light with $\lambda > 420$ nm could not excite BiOCl to produce hydroxyl radicals because of its large band gap, so the degradation of MO on BiOCl may mainly proceed in a photosensitization pathway under visible light irradiation. We proposed that the degradation of MO on BiOCl might also mainly proceed in the photosensitization pathway under UV−vis light irradiation. This is because the decrease on the degradation ratios of MO was a mere 2% for BiOCl when the light source was changed from UV−vis light to visible light. However, it is difficult to find out which pathway is dominant for the degradation of MO on BiOBr and BiOI because both of them could be excited by both UV−vis and visible light with $\lambda > 420$ nm.

4. Conclusions

In summary, we have synthesized hierarchical BiOX (X = Cl, Br, I) nanoplate microspheres by a general one-pot solvothermal process. Ethylene glycol was found to not only act as the reaction medium but also play an important role in the formation of hierarchical BiOX nanoplate microspheres. On the basis of characterizations, we proposed a possible process for the growth of hierarchical BiOX nanoplate microspheres. Moreover, we compared the photocatalytic activities of BiOX on the degradation of methyl orange under UV−vis and visible light irradiation ($\lambda > 420$ nm) and found that BiOI exhibited the best photocatalytic activity among the three BiOX hierarchical nanoplate microspheres because of its suitable band gap. The resulting hierarchical BiOX nanoplate microspheres are very promising photocatalysts for degrading organic pollutants and other applications.

Acknowledgment. This work was supported by National Basic Research Program of China (973 Program) (Grant 2007CB613301), National Science Foundation of China (Grants 20673041, 20503009, and 20777026), Program for New Century Excellent Talents in University, Open Fund of Key Laboratory of Catalysis and Materials Science of the State Ethnic Affairs Commission & Ministry of Education, Hubei Province (Grants CHCL0508 and CHCL06012), and Postdoctors Foundation of China (Grants 20070410935).

Supporting Information Available: XRD patterns and SEM micrographs of BiOX (X = Cl, Br, I) powders prepared by hydrothermal process. The material is available free of charge via the Internet at http://pubs.acs.org.

References and Notes

(1) Vayssieres, L.; Keis, K.; Hagfeldt, A.; Lindquist, S. E. *Chem. Mater.* **2001**, *13*, 4395.

(2) Greene, L. E.; Law, M.; Goldberger, J.; Kim, F.; Johnson, J. C.; Zhang, Y. F.; Saykally, R. J.; Yang, P. D. *Angew. Chem., Int. Ed.* **2003**, *42*, 3031.

(3) Viravaidya, C.; Li, M.; Mann, S. *Chem. Commun.* **2004**, *19*, 2182.

(4) Yu, S. H.; Colfen, H.; Antonietti, M. *Chem.−Eur. J.* **2002**, *8*, 2937.

(5) Demazeau, G. *J. Mater. Chem.* **1999**, *9*, 15.

(6) Yin, S.; Uchida, S.; Fujishiro, Y.; Aki, M.; Sato, T. *J. Mater. Chem.* **1999**, *9*, 1191.

(7) Rabenau, A. *Angew. Chem., Int. Ed. Engl.* **1985**, *24*, 1026.

(8) Li, J.; Chen, Z.; Wang, R. J.; Proserpio, D. M. *Coord. Chem. Rev.* **1999**, *190*, 707.

(9) Toneguzzo, P.; Viau, G.; Acher, O.; Fievet-Vincent, F.; Fievet, F. *Adv. Mater.* **1998**, *10*, 1032.

(10) Sun, Y. G.; Xia, Y. N. *Adv. Mater.* **2002**, *14*, 833.

(11) Merikhi, J.; Jungk, H. O.; Feldmann, C. *J. Mater. Chem.* **2000**, *10*, 1311.

(12) Feldmann, C.; Jungk, H. O. *Angew. Chem., Int. Ed.* **2001**, *40*, 359.

(13) Li, Q.; Ding, Y.; Li, F. Q.; Xie, B.; Qian, Y. T. *J. Cryst. Growth* **2002**, *236*, 357.

(14) Wang, Y. L.; Xia, Y. N. *Nano Lett.* **2004**, *4*, 2047.

(15) Sun, X. M.; Li, Y. D. *Angew. Chem., Int. Ed.* **2004**, *43*, 3827.

(16) Kusainova, A. M.; Zhou, W. Z.; Irvine, J. T. S.; Lightfoot, P. *J. Solid State Chem.* **2002**, *166*, 148.

(17) Burch, R.; Chalker, S.; Loader, P.; Thomas, J. M.; Ueda, W. *Appl. Catal., A* **1992**, *82*, 77.

(18) Kijima, N.; Matano, K.; Saito, M.; Oikawa, T.; Konishi, T.; Yasuda, H.; Sato, T.; Yoshimura, Y. *Appl. Catal., A* **2001**, *206*, 237.

(19) Kusainova, A. M.; Lightfoot, P.; Zhou, W.; Stefanovich, S. Y.; Mosunov, A. V.; Dolgikh, V. A. *Chem. Mater.* **2001**, *13*, 4731.

(20) Charkin, D. O.; Berdonosov, P. S.; Moisejev, A. M.; Shagiakhmetov, R. R.; Dolgikh, V. A.; Lightfoot, P. *J. Solid State Chem.* **1999**, *147*, 527.

(21) Maile, F. J.; Pfaff, G.; Reynders, P. *Prog. Org. Coat.* **2005**, *54*, 150.

(22) Zhang, K. L.; Liu, C. M.; Huang, F. Q.; Zheng, C.; Wang, W. D. *Appl. Catal., B* **2006**, *68*, 125.

(23) Lin, X. P.; Huang, T.; Huang, F. Q.; Wang, W. D.; Shi, J. L. *J. Phys. Chem. B* **2006**, *110*, 24629.

(24) Zhou, S. X.; Ke, Y. X.; Li, J. M.; Lu, S. M. *Mater. Lett.* **2003**, *57*, 2053− 2055.

(25) Henle, J.; Simon, P.; Frenzel, A.; Scholz, S.; Kaskel, S. *Chem. Mater.* **2007**, *19*, 366.

(26) Wang, Y.; Jiang, Y.; Xia, Y. *J. Am. Chem. Soc.* **2003**, *125*, 16176.

(27) Chen, J.; Herricks, T.; Geissler, M.; Xia, Y. N. *J. Am. Chem. Soc.* **2004**, *126*, 10854.

(28) Yu, D. B.; Sun, X. Q.; Zou, J. W.; Wang, Z. R.; Wang, F.; Tang, K. *J. Phys. Chem. B* **2006**, *110*, 21667.

(29) Butler, M. A. *J. Appl. Phys.* **1977**, *48*, 1914.

(30) Ren, W. J.; Ai, Z. H.; Jia, F. L.; Zhang, L. Z.; Fan, X. X.; Zou, Z. G. *Appl. Catal., B* **2007**, *69*, 138.

(31) Kubelka, P. S.; Munk, F. *Z. Tech. Phys.* **1931**, *12*, 593.